Evaluation of discretization schemes for advection-diffusion equations

B. Koren, C.B. Vreugdenhil

Department of Numerical Mathematics

Report NM-R9311 July 1993

CWI is the National Research Institute for Mathematics and Computer Science. CWI is part of the Stichting Mathematisch Centrum (SMC), the Dutch foundation for promotion of mathematics and computer science and their applications.
SMC is sponsored by the Netherlands Organization for Scientific Research (NWO). CWI is a member of ERCIM, the European Research Consortium for Informatics and Mathematics.

P.O. Box 94079, 1090 GB Amsterdam (NL)
Kruislaan 413, 1098 SJ Amsterdam (NL)
Telephone +31 20 592 9333
Telefax +31 20 592 4199

Evaluation of Discretization Schemes for Advection-Diffusion Equations

B. Koren
CWI
P.O. Box 4079, 1009 AB Amsterdam, The Netherlands

C.B. Vreugdenhil
IMAU
P.O. Box 80.005, 3508 TA Utrecht, The Netherlands

Abstract

A comparative study is made of accuracy, monotonicity, conservation, and computational efficiency, for a wide variety of advection-diffusion schemes. The evaluation is based on a set of scalar test problems with known exact solutions: an unsteady, linear 1-D advection-diffusion problem, a steady, linear 1-D advection-diffusion problem with source term, an unsteady, nonlinear 1-D advection problem (with and without discontinuity), and an unsteady, linear 2-D advection problem.

1991 Mathematics Subject Classification: 65Mxx, 65Nxx.
Keywords and Phrases: discretization of advection, diffusion and source terms; pollutant transport.
Note: This report is an extended version of [12]. The evaluation reported was partly performed in the framework of the project CIRK, belonging to CWI's research program "Mathematics & the Environment".

1 Introduction

In this report, quantitative and qualitative comparisons are made between various types of discretization methods for advection-diffusion equations. The comparisons are made on the basis of numerical results obtained for the five test problems defined in [1]. The problem specifications are repeated here.

1.1 Test problems

1.1.1 Problem 1

In this problem, 1-D advection-diffusion of a pollutant is considered. The initial-boundary value problem reads:

$$\frac{\partial c}{\partial t} + u\frac{\partial c}{\partial x} - D\frac{\partial^2 c}{\partial x^2} = 0, \quad x \in [0,1], \tag{1a}$$

$$\begin{aligned} c(x,t=0) &= \sin\left(\pi \tfrac{x-a}{b-a}\right), \quad x \in [a,b], \\ c(x,t=0) &= 0, \qquad\qquad\quad x \notin [a,b], \end{aligned} \tag{1b}$$

$$\begin{aligned} c(x=0,t) &= 0, \\ c(x=1,t) &= 0. \end{aligned} \tag{1c}$$

Data given are: $u = 1$, $D = 0.002$, $a = 0.2$, $b = 0.4$. Requested: $c(x, t = 0.3)$. Note that, in general, the boundary conditions (1c) are sensible only if the pollutant does not reach the boundaries in the given time. Boundary-layer effects therefore do not play an important role in this test problem. The exact solution is known; for details on it we refer to [1]. In Figure 1 we confine ourselves to graphs of

Report NM-R9311
ISSN 0169-0388
CWI
P.O. Box 94079, 1090 GB Amsterdam, The Netherlands

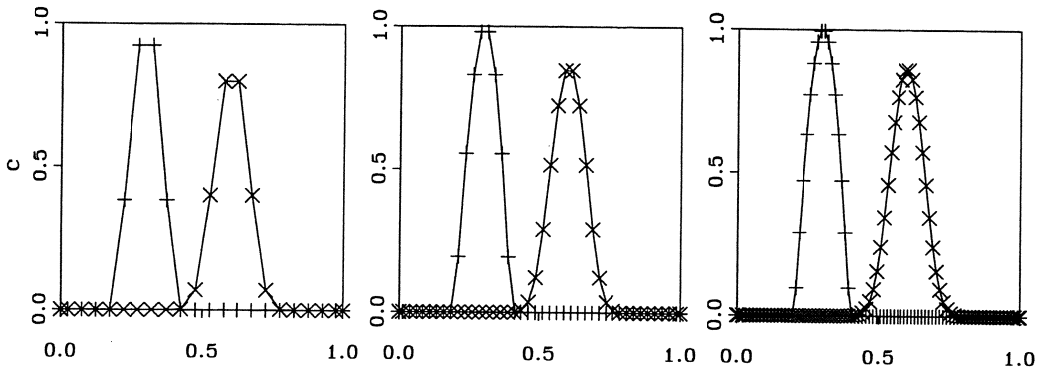

a. $h = \frac{1}{20}$. b. $h = \frac{1}{40}$. c. $h = \frac{1}{80}$.

Figure 1: Solutions Problem 1; +: initial, ×: exact at $t = 0.3$.

the initial and the exact solutions, for the sequence of equidistant, cell-centered finite-volume grids with $h = \frac{1}{20}, \frac{1}{40}, \frac{1}{80}$.

1.1.2 Problem 2

In this problem, 1-D advection-diffusion in steady state and in case of a spatially distributed source, is considered. The problem reads:

$$u\frac{\partial c}{\partial x} - D\frac{\partial^2 c}{\partial x^2} = S(x), \quad x \in [0,1], \tag{2a}$$

with as source:

$$\begin{aligned} S(x) &= \tfrac{\pi}{b-a} u \sin\left(2\pi \tfrac{x-a}{b-a}\right) - \tfrac{2\pi^2}{(b-a)^2} D \cos\left(2\pi \tfrac{x-a}{b-a}\right), && x \in [a,b], \\ S(x) &= 0, && x \notin [a,b], \end{aligned} \tag{2b}$$

and as boundary conditions:

$$\begin{aligned} c(x=0) &= 0, \\ c(x=1) &= 0. \end{aligned} \tag{2c}$$

The source function (2b) has been constructed in such a way that it was easy to arrive at an exact solution. The splitting in an advective part and a diffusive part therefore does not have any physical meaning. Note that the source function is discontinuous at $x = a$ and $x = b$ for $D \neq 0$. (Discontinuous

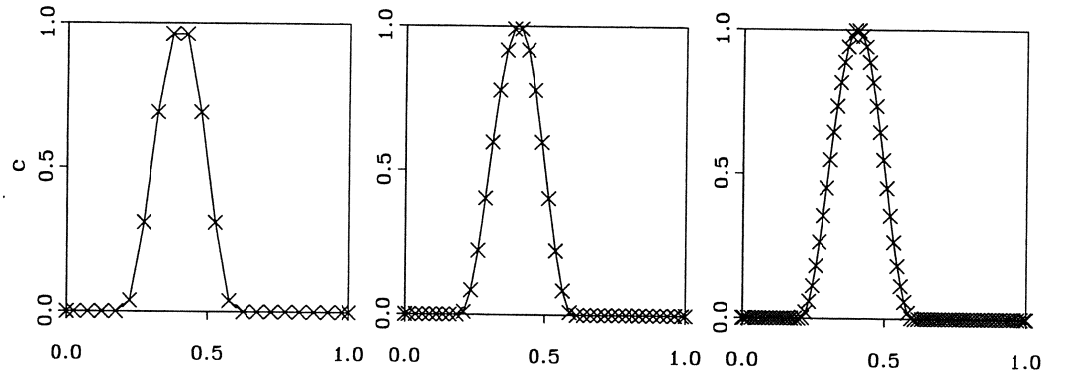

a. $h = \frac{1}{20}$. b. $h = \frac{1}{40}$. c. $h = \frac{1}{80}$.

Figure 2: Exact solutions Problem 2.

sources occur quite often in pollutant transport computations.) As for the boundary conditions, also here it is assumed that no boundary layers occur. The numerical solution $c(x)$ is requested for: $a = 0.2$, $b = 0.6$, $u = 1$, $D = 0.01$. The exact solution is known; see [1] as well as [5]. In Figure 2, on the same sequence of equidistant, cell-centered finite-volume grids as for Problem 1, the exact, discrete solutions are given.

1.1.3 Problems 3.1 and 3.2

For Problem 3, 1-D, nonlinear, unsteady advection is the issue. The nonlinear simple-wave equation

$$\frac{\partial c}{\partial t} + \frac{\partial c^n}{\partial x} = 0, \tag{3a}$$

is considered. For $n = 2$, it is the Burgers equation, and for $n = 5$ a model equation for sediment transport. The initial condition given is:

$$\begin{aligned} c(x, t = 0) &= a - b\cos\left(2\pi\tfrac{x}{L}\right), \quad x \in [0, L], \\ c(x, t = 0) &= a - b, \qquad\qquad\quad x \notin [0, L]. \end{aligned} \tag{3b}$$

Inflow boundary condition is:

$$c(x = 0, t) = a - b. \tag{3c}$$

Two data sets given are: (i) $n = 2$, $a = 1$, $b = 0.01$, $L = 1$, $x \in [0, 4]$ for Problem 3.1, and (ii) $n = 5$, $a = 1$, $b = 0.5$, $L = 1$, $x \in [0, 2]$ for Problem 3.2. Requested in Problem 3.1: $c(x, t = 1)$, and in Problem 3.2: $c(x, t = 0.1)$. For detailed information on the exact solutions, we refer to [1]. In Figures 3 and 4 we confine ourselves again to graphs of initial and exact solutions, here for the sequence of equidistant, cell-centered finite-volume grids with $h = \frac{1}{10}, \frac{1}{20}, \frac{1}{40}$.

1.1.4 Problem 4

For Problem 4, multi-dimensionality is the issue. It describes the 2-D, linear, unsteady advection of a cloud of pollutant. The problem reads:

$$\frac{\partial c}{\partial t} + u\frac{\partial c}{\partial x} + v\frac{\partial c}{\partial y} = 0, \quad (x, y) \in [-1, 1] \times [-1, 1], \tag{4a}$$

with as velocity field:

$$(u, v) = (-\omega y, \omega x), \quad \omega > 0, \tag{4b}$$

as the initial condition:

$$c(x, y, t = 0) = 0.01^{4\left((x+\frac{1}{2})^2+y^2\right)}, \tag{4c}$$

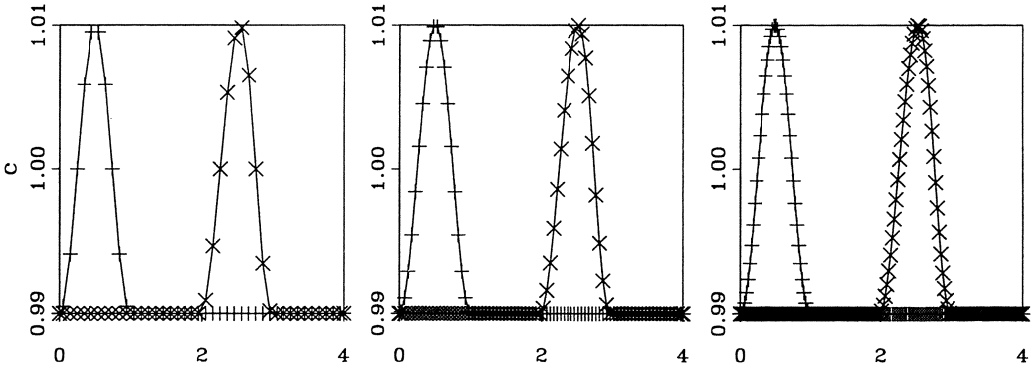

a. $h = \frac{1}{10}$. b. $h = \frac{1}{20}$. c. $h = \frac{1}{40}$.

Figure 3: Solutions Problem 3.1; +: initial, ×: exact at $t = 1$.

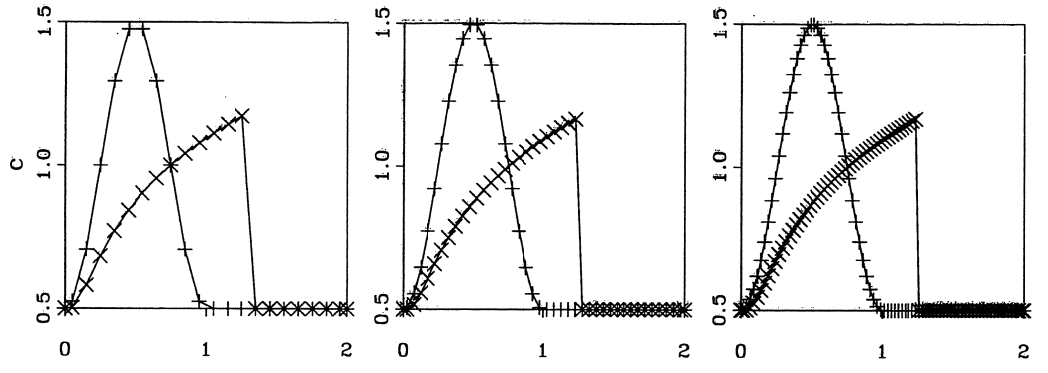

a. $h = \frac{1}{10}$. b. $h = \frac{1}{20}$. c. $h = \frac{1}{40}$.

Figure 4: Solutions Problem 3.2; +: initial, ×: exact at $t = 0.1$.

and as the inflow boundary conditions:

$$\begin{aligned} c(x=-1,y,t) &= 0.01^{4\left((-1+\frac{1}{2}\cos(\omega t))^2+(y+\frac{1}{2}\sin(\omega t))^2\right)}, & y \in [-1,0], \\ c(x=1,y,t) &= 0.01^{4\left((1+\frac{1}{2}\cos(\omega t))^2+(y+\frac{1}{2}\sin(\omega t))^2\right)}, & y \in [0,1], \\ c(x,y=-1,t) &= 0.01^{4\left((x+\frac{1}{2}\cos(\omega t))^2+(-1+\frac{1}{2}\sin(\omega t))^2\right)}, & x \in [0,1], \\ c(x,y=1,t) &= 0.01^{4\left((x+\frac{1}{2}\cos(\omega t))^2+(1+\frac{1}{2}\sin(\omega t))^2\right)}, & x \in [-1,0]. \end{aligned} \tag{4d}$$

Given: $\omega = 2\pi$, requested: $c(x,y,t=1)$. The problem describes the counter-clockwise solid-body rotation of the Gaussian initial distribution (4c). The numerical solution requested is that after one rotation. The exact solution is identical to initial solution (4c). Graphs of the exact solution are given in Figure 5, for equidistant, cell-centered finite-volume grids with successively 22×21, 42×41 and 82×81 cells, in x- and y-direction, respectively. (These dimensions allow an exact capturing of the local maximum in the initial solution.) Iso-lines are given at $c = 10^{-5} + 0.1n$, $n = 0, 1, \ldots, 9$. The iso-line $c = 10^{-5}$ has been dashed.

1.2 Discretization methods

The types of discretization methods to be evaluated are described in [2-11] and listed in Table 1. (In most of the references [2-11], more than one specific discretization method is considered.) We start by making quantitative comparisons. For this purpose, we have in principle selected a single discretization method from each of the ten references [2-11]. The selected methods are compared on the

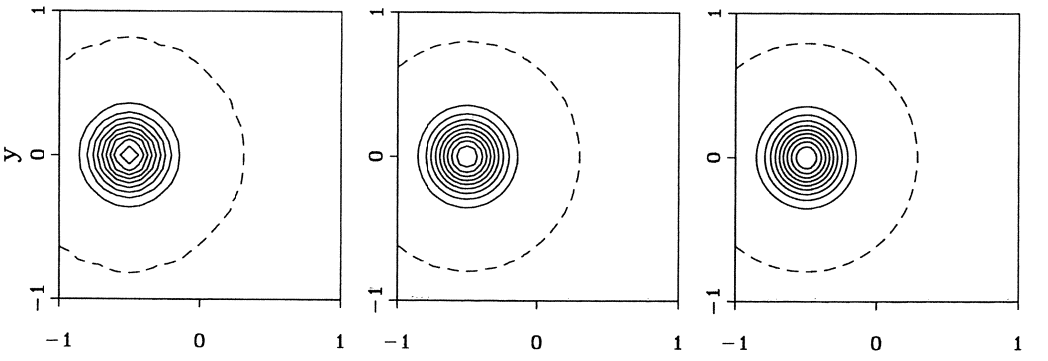

a. 22×21-grid. b. 42×41-grid. c. 82×81-grid.

Figure 5: Exact solutions Problem 4.

Reference	*method(s)*
[2]	linear, central finite differences (standard second-order and compact higher-order)
[3]	linear, upwind finite differences (grid-aligned and rotated) and upwind finite volumes
[4]	classical nonlinear, upwind finite volumes
[5]	modern nonlinear, upwind finite volumes
[6]	ENO, finite differences (standard and variable order)
[7]	spectral (standard spectral and spectral elements)
[8]	finite elements (standard Galerkin and streamline upwind Petrov-Galerkin)
[9]	backward semi-Lagrangian
[10]	forward semi-Lagrangian
[11]	fluctuation-splitting

Table 1: Types of discretization methods considered in [2-11].

basis of the numerical results presented for Problem 4. Reliable quantitative comparisons are possible for this problem, because of its smoothness, its well-specified output data, its prescribed sequence of grids: $\sim (20 \times 20), \sim (40 \times 40), \sim (80 \times 80)$, and because of its prescribed benchmark problem for measuring computing times. After this quantitative comparison, partly quantitative - partly qualitative comparisons are made on the basis of the numerical results obtained for Problems 1, 2, 3.1, and 3.2. For these comparisons, per problem we have in principle also selected a single discretization method from each of the References [2-11]. Interesting difficulties of the latter four problems are the local non-smoothnesses in initial solutions and source terms. These non-smoothnesses may result in reduced global orders of accuracy.

The present evaluation still reflects our own subjective opinions, be it to a minimal extent. We have aimed at objectivity by giving the authors of the ten references the opportunity to make critical reviews of a draft of the present evaluation.

2 Evaluation numerical results Problem 4

The specific discretization methods selected for the present (quantitative) evaluation, are given in Table 2. For [5, 7, 9, 10], a selection was not necessary; in these references, results for Problem 4 are presented for a single method solely. From [3], because of the rather widely divergent, linear upwind methods considered in it, two specific schemes have been selected. Detailed descriptions of the specific discretization methods are given in the corresponding references. Here we suffice to give very short descriptions only. The leap-frog scheme from [2] is the known, standard leap-frog scheme, which is second-order accurate and central in both space and time. The skew-triangle scheme from [3] is a first-order accurate, rotated, 2-D upwind scheme. The cyclic scheme from [3] uses a two-stage time-integration, with per stage a different space discretization. When the two consecutive stages are considered as one, the favorable numerical properties of each of both schemes are maintained. The MFCT (multi-dimensional flux corrected transport) scheme from [4] is an upwind scheme with limiting procedure for preventing spurious non-monotonicities. The adjective multi-dimensional refers to the fact that in 2-D and 3-D the limiting procedure is simultaneously applied in 2 and 3 dimensions, respectively. The limited - $\kappa = \frac{1}{3}$ scheme from [5] is comparable to the MFCT scheme. Differences are that the underlying, plain $\kappa = \frac{1}{3}$ scheme is third-order accurate (for steady 1-D problems), instead of second-order accurate. Further, the $\kappa = \frac{1}{3}$ limiter is constructed according to more recent theory; besides monotonicity requirements the $\kappa = \frac{1}{3}$ limiter also explicitly satisfies accuracy requirements. The ENO-4-LF scheme from [6] is a fourth-order accurate, global Lax-Friedrichs variant of the standard fourth-order accurate ENO (essentially non-oscillatory) scheme. The SEM scheme from [7] is a Galerkin spectral-element scheme with special time stepping, a combination of forward Euler and Taylor-Galerkin time stepping. The SGA/CN-consistent scheme from [8] is a standard Galerkin finite-element method which uses linear (non-upwinded) interpolation on triangular elements. CN refers to Crank-Nicolson time integration, and the adjective consistent to the fact that the mass matrix is consistent (i.e. that no lumping is applied). The adjoint-equation

method	*Figure/Table*
leap-frog	Figure 2.9 from [2]
skew-triangle	Table 3.6 from [3]
cyclic	Table 3.8 from [3]
MFCT	Tables 4.4-4.7 from [4]
limited - $\kappa = \frac{1}{3}$	Table 5.3 from [5]
ENO-4-LF	Table 6.3b from [6]
SEM	Table 7.6 from [7]
SGA/CN-consistent	Table 8.3 from [8]
adjoint-equation	Table 9.11 from [9]
second-moment	Table 10.1 from [10]
narrow	Figure 11.17 from [11]

Table 2: Specific discretization methods to be evaluated for Problem 4.

method from [9] is a backward semi-Lagrangian method. As a Lagrangian method it tracks the propagation paths of fluid particles (or particles immersed in the fluid). The adjective semi-Lagrangian refers to the fact that, for interpolation purposes, the particles are mapped on a grid. Backward refers to the property that the interpolation on the grid is done at the previous time level (backward in time). The second-moment method from [10] also is a semi-Lagrangian method. In principle, it only differs in the time level at which grid interpolation is done. Here the interpolation, a particle redistribution on the grid, is done at the next time level (forward in time). The narrow scheme from [11], finally, is a first-order accurate, multi-D upwind scheme, which on a grid with triangular cells properly distributes scalar fluctuations to the downstream cell vertices.

The numerical properties to be evaluated are successively: accuracy (both plain accuracy and accuracy in relation to computational efficiency), positivity and conservation. We realize that this choice of numerical properties does not permit a general evaluation. For this, many more properties should be considered: memory use, complexity of implementation, suitability for parallelization and vectorization, applicability of acceleration techniques (such as conjugate gradients and multigrid), suitability for unstructured grids, and so on. In order to make a clear comparison, we restrict ourselves to the few but relevant numerical properties mentioned above.

Plain accuracy is evaluated on the basis of the numerical data obtained for:

$$|1 - c_{\max}| \equiv |1 - (c_{\text{numerical}}(i,j))_{\max}|\,, \tag{5a}$$

$$\|\Delta c\|_1 \equiv \frac{\sum_{i,j} \mid c_{\text{exact}}(i,j) - c_{\text{numerical}}(i,j) \mid}{\sum_{i,j} 1}, \tag{5b}$$

$$\|\Delta c\|_\infty \equiv \mid c_{\text{exact}}(i,j) - c_{\text{numerical}}(i,j) \mid_{\max}\,. \tag{5c}$$

Accuracy in relation to computational efficiency is studied by means of $\|\Delta c\|_1$ versus normalized CPU-time. Positivity and conservation are studied by, respectively:

$$|c_{\min}| \equiv |(c_{\text{numerical}}(i,j))_{\min}|\,, \tag{6}$$

and

$$|1 - r_{\text{mass}}| \equiv \left| 1 - \frac{\sum_{i,j} c_{\text{numerical}}(i,j)}{\sum_{i,j} c_{\text{exact}}(i,j)} \right|. \tag{7}$$

All numerical results, except those of the spectral-element scheme, have been obtained on a sequence of three grids with as minimal numbers of points (or cells): $(n_x \times n_y) = (20 \times 20), (40 \times 40), (80 \times 80)$, and with as maximal numbers: $(n_x \times n_y) = (22 \times 21), (42 \times 41), (82 \times 81)$. The fineness of the sequence of three space discretizations as used by the spectral-element method, $(n_e, n) = (4,4), (4,8), (4,16)$ with n_e the number of non-overlapping elements into which the computational domain is broken up and

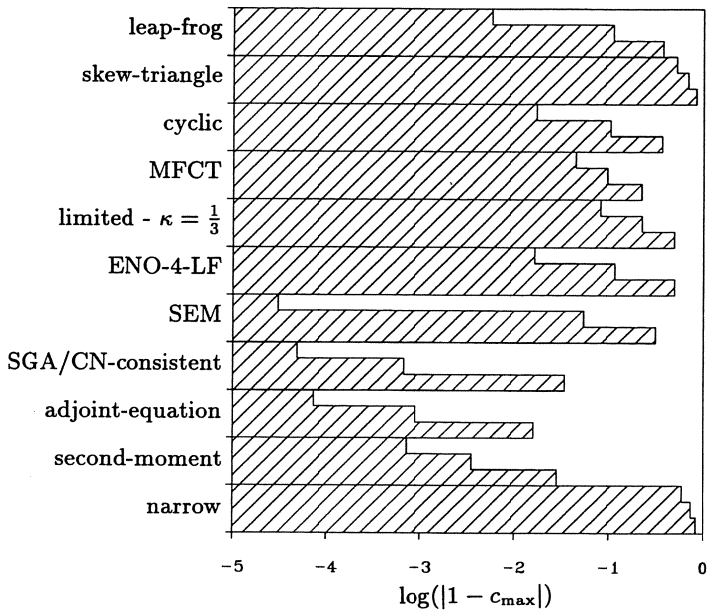

Figure 6: Values of $|1 - c_{\max}|$, for prescribed grid sequence and selected discretization methods.

with n the degree of the interpolation polynomial, can be considered to be equivalent to that of the grid sequence $(n_x \times n_y) = (9 \times 9), (17 \times 17), (33 \times 33)$. Another remark that needs to be made in advance concerns the treatment of the velocity field by the semi-Lagrangian methods from [9, 10]. Both methods use exact characteristic information. (The adjoint-equation method from [9] directly uses the exact characteristics. The second-moment method from [10] uses a numerical method in computing the characteristics, but for the present solid-body-like rotation, this numerical method boils down to the use of exact characteristic information as well.) The possibility to use exact characteristic information, if available, definitely is an advantage over Eulerian discretization methods. However, in general, exact information is lacking and it is not sufficiently clear to what extent this absence will detract from the accuracy and computational efficiency of semi-Lagrangian methods.

2.1 Plain accuracy

2.1.1 Peak resolution

Peak resolution is measured on the basis of $|1 - c_{\max}|$. Its values, as measured for the selected discretization methods (Table 2), are given in Figure 6. Per method we depict in upward direction: the values measured on the coarsest, the medium-sized and the finest grid. In addition, in Table 3, we give per method the average error value $\overline{|1 - c_{\max}|}$ over the three grids. In case of $(n_x \times n_y) = (20 \times 20), (40 \times 40), (80 \times 80)$, this means $\overline{|1 - c_{\max}|} = \frac{1}{3}\Big(|1 - c_{\max}|_{(n_x \times n_y)=(20\times 20)} + |1 - c_{\max}|_{(n_x \times n_y)=(40\times 40)} + |1 - c_{\max}|_{(n_x \times n_y)=(80\times 80)}\Big)$. To be able to make a reasonable comparison, for the spectral-element scheme we take $\overline{|1 - c_{\max}|} = \frac{1}{2}\Big(|1 - c_{\max}|_{(n_e,n)=(4,8)} + |1 - c_{\max}|_{(n_e,n)=(4,16)}\Big)$. (For $\overline{\|\Delta c\|_\infty}$, $\overline{\|\Delta c\|_1}$, $\overline{|c_{\min}|}$ and $\overline{|1 - r_{\text{mass}}|}$, the same averagings will be made.) Furthermore, in Table 3 we give the orders of accuracy p (p from $\mathcal{O}(h^p)$), as measured from the medium-sized grid to the finest grid. (In the following, this way of measuring orders of accuracy will also be applied to $\|\Delta c\|_\infty$, $\|\Delta c\|_1$, $|c_{\min}|$, and $|1 - r_{\text{mass}}|$.) With respect to both error level and error convergence, the methods have been ordered in Table 3 with increasing performance in upward direction. Moreover, by means of horizontal lines, a classification has been made into three categories, say: (i) less good, (ii) good, and (iii) very good. (This type of

error level		*error convergence*	
method	$\overline{\lvert 1 - c_{\max} \rvert}$	*method*	p
adjoint-equation	0.006	SEM	10.8
second-moment	0.011	leap-frog	4.3
SGA/CN-consistent	0.012	SGA/CN-consistent	3.8
SEM	0.027	adjoint-equation	3.6
MFCT	0.119	ENO-4-LF	2.8
cyclic	0.159	cyclic	2.6
leap-frog	0.161	second-moment	2.3
ENO-4-LF	0.204	limited - $\kappa = \frac{1}{3}$	1.5
limited - $\kappa = \frac{1}{3}$	0.260	MFCT	1.1
skew-triangle	0.667	skew-triangle	0.4
narrow	0.707	narrow	0.3

Table 3: Classifications of discretization methods with respect to $\overline{\lvert 1 - c_{\max} \rvert}$.

classification will also be applied to the other four errors.)

We here classify schemes which still have a peak decrease of more than 10 % on the finest grid as low-accurate. We see there are two such schemes: the narrow scheme and the skew-triangle scheme. Concerning the order of accuracy with respect to $\overline{\lvert 1 - c_{\max} \rvert}$, we see that for both schemes this is still below the (theoretically expected) asymptotic $\mathcal{O}(h)$ convergence. Note, however, that for steady multi-D problems the narrow scheme, and particularly the associated PSI scheme, perform significantly better than for unsteady problems (see [11] for evidence on this.) Probably this relatively better performance for steady problems also holds for the skew-triangle scheme. Good results are obtained by the MFCT scheme and the limited - $\kappa = \frac{1}{3}$ scheme, for error level as well as for error convergence. (With respect to average error level, the MFCT scheme is preferable to the limited - $\kappa = \frac{1}{3}$ scheme, with respect to order behavior it is the reverse.) On average, both methods behave more or less the same. Given the comparable numerical recipes in the two methods, this was to be expected. Good to very good orders of accuracy are obtained by the two semi-Lagrangian schemes, the cyclic scheme, the ENO scheme, the finite-element scheme, the leap-frog scheme, and the spectral-element scheme. All seven methods have a higher than $\mathcal{O}(h^2)$ accuracy behavior, particularly the spectral-element scheme has a very high order of accuracy. It is followed at great distance by the leap-frog scheme, which is closely followed by the finite-element scheme, the latter having the additional advantage (over the leap-frog scheme) of a very small average error level. As for the superior average peak resolution of the adjoint-equation method, it is unfortunately not clear to what extent this is favored by the direct use of exact characteristic information. The remaining results speak for themselves.

2.1.2 L_∞-norm solution error

We proceed by considering $\|\Delta c\|_\infty$, which for many methods is supposed to be closely related to $\overline{\lvert 1 - c_{\max} \rvert}$. The values of $\|\Delta c\|_\infty$, as measured for the selected methods, are given in Figure 7. As in Figure 6, depicted upward per method are: the values measured on the coarsest, the medium-sized and the finest grid. Furthermore, as in Table 3, in Table 4 we also give the classifications for average error levels and orders of accuracy.

The skew-triangle scheme and the narrow scheme appear to behave much the same again. Here also, the orders of accuracy of both schemes are still below $\mathcal{O}(h)$. Good order behavior is shown by the MFCT scheme, the limited - $\kappa = \frac{1}{3}$ scheme, the leap-frog scheme, the adjoint-equation scheme, and the cyclic scheme. All five schemes behave in between $\mathcal{O}(h)$ and $\mathcal{O}(h^2)$. Note the excellent average error level of the adjoint-equation method. Higher than second-order accuracy is shown again by the second-moment scheme, the ENO scheme, the finite-element scheme, and (the best again) by the spectral-element scheme.

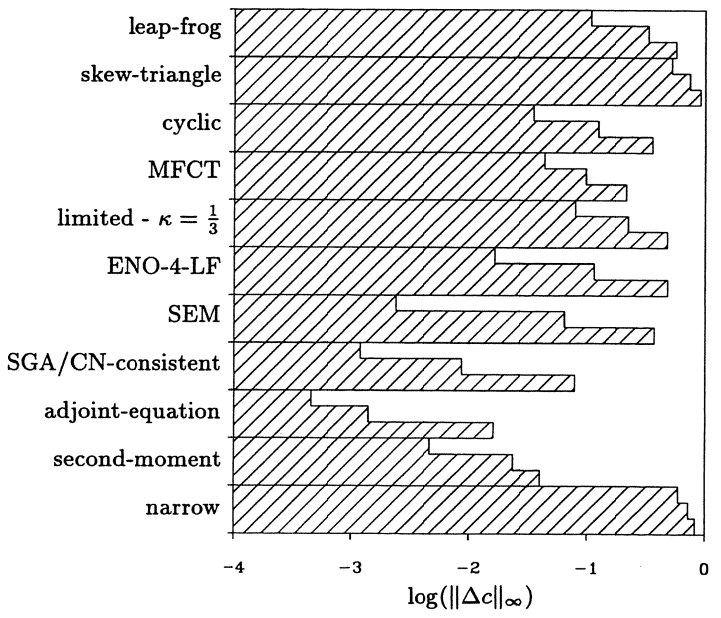

Figure 7: Values of $\|\Delta c\|_\infty$, for prescribed grid sequence and selected discretization methods.

error level		*error convergence*	
method	$\overline{\|\Delta c\|_\infty}$	*method*	p
adjoint-equation	0.006	SEM	4.8
second-moment	0.023	SGA/CN-consistent	2.9
SGA/CN-consistent	0.030	ENO-4-LF	2.8
SEM	0.034	second-moment	2.3
MFCT	0.119	cyclic	1.8
cyclic	0.172	leap-frog, adjoint-equation	1.6
ENO-4-LF	0.204	limited - $\kappa = \frac{1}{3}$	1.5
limited - $\kappa = \frac{1}{3}$	0.261	MFCT	1.2
leap-frog	0.333	skew-triangle	0.5
narrow	0.710	narrow	0.3
skew-triangle	0.723		

Table 4: Classifications of discretization methods with respect to $\|\Delta c\|_\infty$.

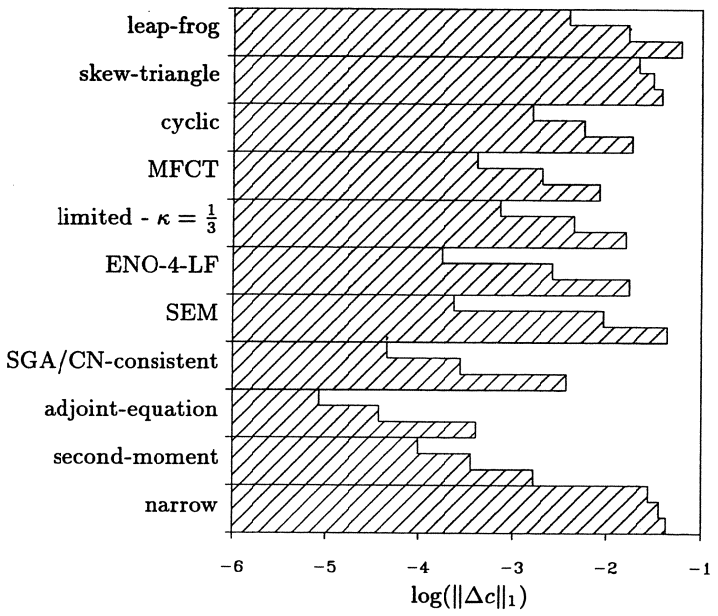

Figure 8: Values of $\|\Delta c\|_1$, for prescribed grid sequence and selected discretization methods.

2.1.3 L_1-norm solution error

We end this evaluation of plain accuracy by considering $\|\Delta c\|_1$. The values measured for it are given in Figure 8. Classifications are given in Table 5.

We observe that here also the skew-triangle scheme and the narrow scheme have an order of accuracy which is still lower than $\mathcal{O}(h)$, with the skew-triangle scheme again converging slightly better than the narrow scheme. A nearly $\mathcal{O}(h^2)$ accuracy behavior is obtained by the cyclic scheme and the second-moment scheme. All remaining schemes show a higher than $\mathcal{O}(h^2)$ behavior. A superior order of accuracy is shown again by the spectral-element scheme. The solution error of the limited - $\kappa = \frac{1}{3}$ scheme converges a little faster again than that of the MFCT scheme, whereas the average error level of the MFCT scheme is somewhat lower again than that of the limited - $\kappa = \frac{1}{3}$ scheme. The ENO scheme practically reaches its $\mathcal{O}(h^4)$ accuracy behavior in going from the medium-sized grid to the finest grid. Yet, note the modest error level of the ENO scheme on the coarsest grid. High-resolution schemes as this ENO scheme (and in some sense also the limited - $\kappa = \frac{1}{3}$ scheme) seem to need sufficient smoothness and distance from boundaries; i.e. sufficient grid fineness. However, note also that this does *not* seem to be the case for the variable-order ENO schemes introduced in [6] (not depicted in Figure 8), nor for the spectral-element scheme (Figure 8). (Concerning the variable-order ENO schemes, compare the coarsest-grid value of $\|\Delta c\|_1$, as given in Table 6.6 from [6], with the corresponding ENO-4-LF value given in Table 6.3b from [6]. As for the spectral-element scheme, we emphasize again that its results for the medium-sized resolution $(n_e, n) = (4, 8)$ should be compared with the coarsest-grid results of all other methods $(n_x \times n_y) \approx (20 \times 20)$.) Excellent coarse-grid resolution is also shown by the Galerkin finite-element scheme and by the two semi-Lagrangian schemes. For the latter two schemes, this can probably be attributed in large measure to their use of exact characteristic information; for the finite-element scheme it is not well-understood, however.

2.2 Accuracy versus computational efficiency

Accuracy in relation to computational costs is studied by means of the $\|\Delta c\|_1$-values and normalized CPU-times. Normalization of CPU-times measured by the different authors, has been achieved by means of a benchmark code, the code for the computation of Problem 4 on a 40 × 40-grid, by the leap-frog

error level		*error convergence*	
method	$\overline{\|\Delta c\|_1}$	*method*	p
adjoint-equation	1.5×10^{-4}	SEM	5.3
second-moment	7.0×10^{-4}	ENO-4-LF	3.9
SGA/CN-consistent	1.4×10^{-3}	limited - $\kappa = \frac{1}{3}$, SGA/CN-consistent	2.6
MFCT	3.6×10^{-3}	MFCT	2.3
SEM	4.8×10^{-3}	adjoint-equation	2.2
ENO-4-LF	6.7×10^{-3}	leap-frog	2.1
limited - $\kappa = \frac{1}{3}$	7.0×10^{-3}	cyclic, second-moment	1.9
cyclic	8.6×10^{-3}	skew-triangle	0.5
leap-frog	2.7×10^{-2}	narrow	0.4
skew-triangle	3.0×10^{-2}		
narrow	3.6×10^{-2}		

Table 5: Classifications of discretization methods with respect to $\|\Delta c\|_1$.

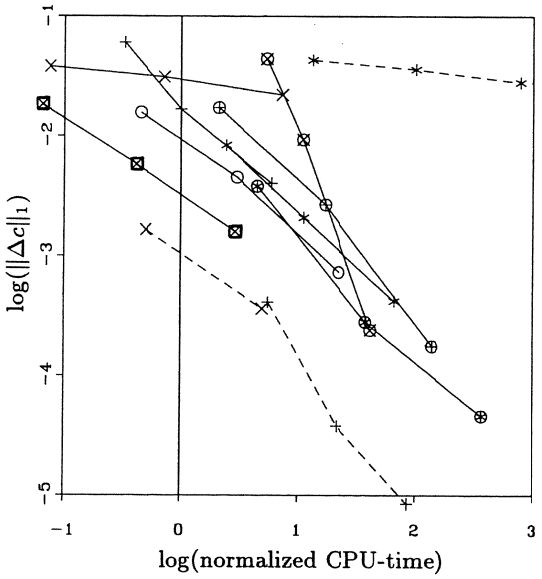

Figure 9: Values of $\|\Delta c\|_1$ versus normalized CPU-times for prescribed grid sequence and selected discretization methods; **solid lines**: $+$: leap-frog, $\times$: skew-triangle, $\boxtimes$: cyclic, $*$: MFCT, $\bigcirc$: limited - $\kappa = \frac{1}{3}$, $\oplus$: ENO-4-LF, $\otimes$: SEM, $\circledast$: SGA/CN-consistent; **dashed lines**: $+$: adjoint-equation, $\times$: second-moment, $*$: narrow.

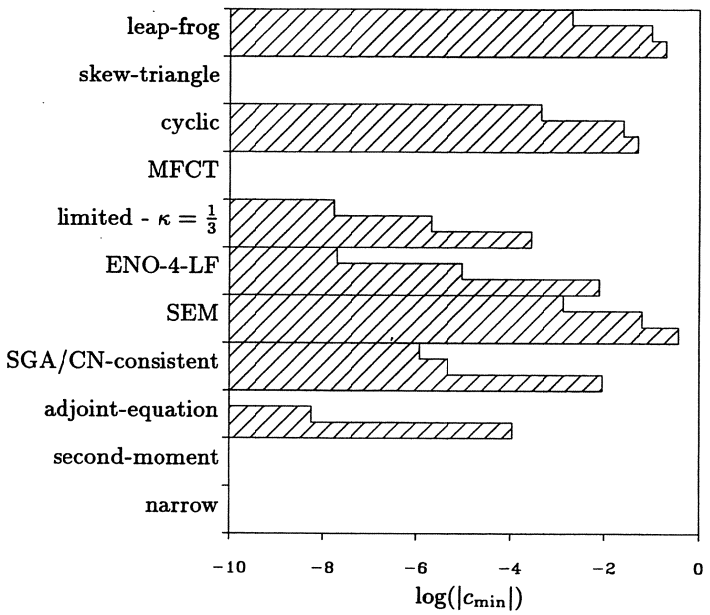

Figure 10: Values of $|c_{min}|$, for prescribed grid sequence and selected discretization methods.

method from [2]. Since the authors have used different time integrators which also differ in degree of optimization, the importance of the present evaluation should not be overestimated of course. Still we think that the results do give some reliable qualitative information about the price-performance aspects of the various space discretization methods.

In Figure 9 the results are given. The measured data of the two semi-Lagrangian schemes (the adjoint-equation method and the second-moment method) as well as the data of the narrow scheme have been set apart from those of the other schemes by connecting them with dashed lines. The narrow scheme differs from the other schemes because it has been implemented in a research code meant for unstructured grids, and the two semi-Lagrangian schemes differ because their use of exact characteristic information influences both accuracy and computational efficiency in a positive way. Ignoring this advantage of semi-Lagrangian schemes for (at least) the present sequence of grids, the two schemes definitely appear to be the best buy. Clearly the best performance of all remaining Eulerian schemes is obtained by the cyclic scheme. It is followed by a cluster of higher than first-order Eulerian methods. From these, the limited - $\kappa = \frac{1}{3}$ scheme and the finite-element scheme perform best. The best scheme for grids finer than the present ones seems to be the spectral-element scheme. It appears that, for perfectly smooth problems, a very high order of spatial accuracy is really useful on finer grids (with the restriction, of course, that the accuracy in time is of very high order as well). Also noteworthy is the performance for grids which are *coarser* than those of the sequence considered here. For these coarse grids, the price-performance behavior of low-order schemes, such as the skew-triangle scheme, becomes interesting. This is relevant for e.g. multigrid computations.

2.3 Positivity

Positivity is evaluated on the basis of $|c_{min}|$. The values of $|c_{min}|$, as measured on the sequence of grids for the selected discretization methods, are given in Figure 10. (In Figure 10, no results are missing; all invisible results are smaller than 10^{-10}.) Classifications are given in Table 6.

Relatively poor order behavior is shown by the finite-element scheme. A poor average error level is obtained by the leap-frog scheme, closely followed by the spectral-element scheme and the cyclic scheme. Good average error levels are obtained by the limited - $\kappa = \frac{1}{3}$ scheme and the adjoint-equation method,

error level		*error convergence*	
method	$\overline{\lvert c_{\min}\rvert}$	*method*	p
skew-triangle, MFCT, second-moment, narrow	$< 10^{-10}$	ENO-4-LF	8.9
adjoint-equation	3.7×10^{-5}	limited - $\kappa = \frac{1}{3}$	6.9
limited - $\kappa = \frac{1}{3}$	9.4×10^{-5}	cyclic, adjoint-equation	5.8
ENO-4-LF	2.6×10^{-3}	leap-frog	5.6
SGA/CN-consistent	3.0×10^{-3}	SEM	5.5
cyclic	2.5×10^{-2}	SGA/CN-consistent	2.0
SEM	3.3×10^{-2}		
leap-frog	1.0×10^{-1}		

Table 6: Classifications of discretization methods with respect to $|c_{\min}|$.

whereas their orders of convergence may even be qualified as very good. The limited - $\kappa = \frac{1}{3}$ scheme is not perfectly positive because it is not applied near boundaries. (By introducing a single row of virtual cells across the boundaries, and then applying the limited scheme up to and including the boundaries, perfectly positive results would be obtained.) Although their order behaviors with decreasing mesh size are not visible, we assume that for sufficiently small time steps, perfect positivity is guaranteed for the four schemes with $\overline{|c_{\min}|} < 10^{-10}$. (For the skew-triangle scheme and the narrow scheme, this is certainly the case.) In conclusion, we emphasize that the present problem is in fact not very discriminating with respect to the positivity property; more discriminating are Problem 3.1 and - particularly - Problem 3.2 (to be evaluated in the Sections 3.3 and 3.4).

2.4 Conservation

Whereas the exact net flux across the entire boundary is zero, the local fluxes are not. Although very small, at (almost) all boundary points there is an inflow or outflow flux. As a consequence, when in a numerical computation the exact fluxes are imposed as inflow boundary conditions and when - mathematically correct - no outflow boundary conditions are imposed, due to discretization errors, the net flux across the entire boundary generally will not be equal to zero. Hence, schemes which are strictly conservative, do not show strictly conservative behavior for this test case, unless - mathematically incorrect - the exact fluxes are also imposed at outflow. Nevertheless, poor conservation properties *can* be detected; for schemes which converge well with respect to $\|\Delta c\|_1$ but not so well with respect to $|1 - r_{\text{mass}}|$, it may be concluded that they have poor conservation properties. For a well-conservative scheme, $|1 - r_{\text{mass}}|$ should converge better, the same, or a little bit worse than $\|\Delta c\|_1$, but *not* much (say one or more orders) worse. Hence, a good quantity to look at here is the measured order of accuracy of $|1 - r_{\text{mass}}|$ subtracted by the corresponding measured order of $\|\Delta c\|_1$. The values of $|1 - r_{\text{mass}}|$ as measured on the sequence of grids for the selected discretization methods, are given in Figure 11. Classifications are given in Table 7. In this table, per method, we give the aforementioned order-of-accuracy difference $p_{|1-r_{\text{mass}}|} - p_{\|\Delta c\|_1}$, where $p_{\|\Delta c\|_1}$ has already been given in Table 5.

Schemes of which the order of $|1 - r_{\text{mass}}|$ behaves clearly less well than that of $\|\Delta c\|_1$, are: the second-moment, leap-frog, MFCT, and ENO schemes. All remaining schemes behave well. Still note the good convergence of the narrow scheme. This good performance is explained by the low crosswind-diffusion of that scheme.

2.5 Synopsis

Table 8 collects all preceding classifications of accuracy, efficiency, positivity, and conservation. Here ++ may be interpreted as very good, + as good, and − as less good. In the evaluation of accuracy versus computational efficiency, the two semi-Lagrangian schemes and the narrow scheme have been left

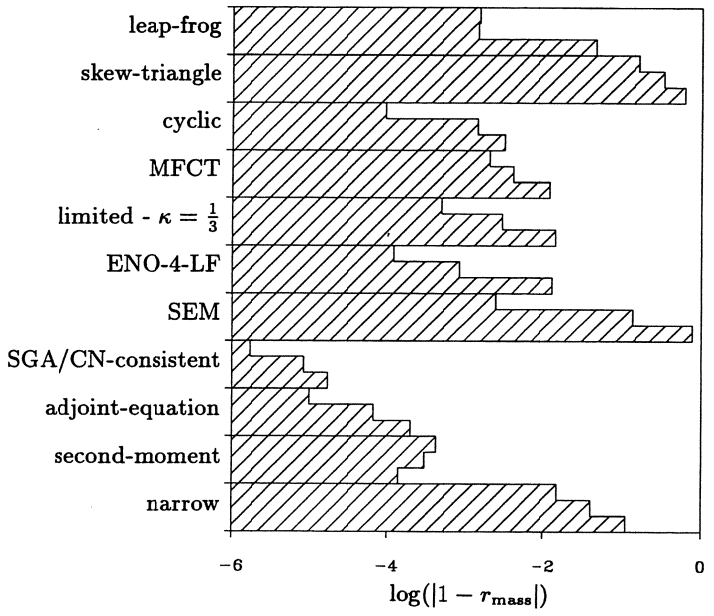

Figure 11: Values of $|1 - r_{\text{mass}}|$, for prescribed grid sequence and selected discretization methods.

error level		*relative error convergence*	
method	$\overline{\lvert 1 - r_{\text{mass}} \rvert}$	*method*	$p_{\lvert 1-r_{\text{mass}} \rvert} - p_{\lVert \Delta c \rVert_1}$
SGA/CN-consistent	9.0×10^{-6}	cyclic	2.0
adjoint-equation	9.2×10^{-5}	narrow	1.0
second-moment	2.9×10^{-4}	adjoint-equation	0.6
cyclic	1.5×10^{-3}	SEM, skew-triangle	0.5
ENO-4-LF	4.6×10^{-3}	limited - $\kappa = \frac{1}{3}$	0.0
limited - $\kappa = \frac{1}{3}$	5.9×10^{-3}	SGA/CN-consistent	−0.3
MFCT	6.0×10^{-3}	ENO-4-LF	−1.1
leap-frog	1.6×10^{-2}	MFCT	−1.3
narrow	5.5×10^{-2}	leap-frog	−2.2
SEM	6.8×10^{-2}	second-moment	−2.4
skew-triangle	3.7×10^{-1}		

Table 7: Classifications of discretization methods with respect to $|1 - r_{\text{mass}}|$.

Reference	*method*	*accuracy*	*accuracy versus CPU-time*	*positivity*	*conservation*
[2]	leap-frog	+	+	−	−
[3]	skew-triangle	−	−	++	−
[3]	cyclic	+	++	−	+
[4]	MFCT	+	+	++	−
[5]	limited - $\kappa = \frac{1}{3}$	+	+	+	+
[6]	ENO-4-LF	++	+	+	−
[7]	SEM	++	+	−	+
[8]	SGA/CN-consistent	++	+	−	++
[9]	adjoint-equation	++	left out	++	++
[10]	second-moment	++	left out	++	+
[11]	narrow	−	left out	++	+

Table 8: Specific discretization methods and their evaluation for Problem 4.

out for reasons explained in Section 2.2.

3 Evaluation numerical results Problems 1, 2, 3.1, and 3.2

Extensive quantitative evaluations are not possible for these four 1-D problems (because no explicit request has been made for quantitative results, and also because no specific grid sequences have been prescribed). Nevertheless, some interesting partly quantitative - partly qualitative comparisons can be made. In the following, per problem, we look for (as far as we can judge) the 'best' method per reference, and give qualifications on such properties as accuracy (phase errors, resolution of maxima, shocks, ...) and monotonicity (or, if applicable, positivity). Reference [11] is left out here, since it considers multi-D methods and multi-D problems only.

3.1 Problem 1

First, in Table 9 (in the 3rd-5th column), we give our evaluation of numerical results obtained for Problem 1. (In most cases, the name of a method in Table 9 refers to the discretization scheme applied to the advection operator.) We proceed by briefly describing the selected discretization methods. As for advection, the leap-frog method from [2] is in principle the same as that applied to Problem 4; it is central in space and time. Diffusion, however, is not integrated centrally in time, but forwardly (by forward Euler, lagged one time step). The quadratic upwind scheme from [3] is a higher-order accurate, rotated upwind scheme for advection. The cyclic, MFCT, and limited - $\kappa = \frac{1}{3}$ schemes are in principle the same as those evaluated for Problem 4. The upwind biased ENO-6 scheme from [6] is a sixth-order accurate, upwind biased ENO scheme. The remaining advection schemes (SEM, SGA-consistent, adjoint-equation, and second-moment) are essentially the same as those applied to Problem 4. For details about the two new advection schemes to be evaluated here, quadratic upwind and upwind biased ENO-6, we refer to [3] and [6], respectively. In Table 9 the same qualifications are used as before (++: very good, +: good, −: less good). In the last column, as far as available, we also give the order of accuracy with respect to $\|\Delta c\|_1$, as measured from the one-but-finest to the finest grid.

An interesting feature of Problem 1 is that its initial condition has a discontinuous first derivative at two points. Due to these two kinks in the initial solution, no higher than $\mathcal{O}(h^2)$ $\|\Delta c\|_1$ convergence can be expected because, in general, a kink in the initial solution causes an $\mathcal{O}(h)$ error extending over an $\mathcal{O}(h)$ area. Note that the presence of diffusion cannot help to remove the $\mathcal{O}(h^2)$ $\|\Delta c\|_1$-error made in discretizing the initial solution. (Diffusion does make the exact solution C^∞ at $t = 0^+$; if the time integration were started from that moment, there would be no $\mathcal{O}(h^2)$ order barrier.) In spite of this theoretical $\mathcal{O}(h^2)$ order barrier, for the grids considered some of the $\mathcal{O}(h^p)_{p>2}$ methods still seem to reach their theoretical order of accuracy, valid for perfectly smooth problems. However, in Section 6.3 of

method	*Figure*	*phase*	*maximum*	*positivity*	$p_{\|\Delta c\|_1}$
leap-frog	2.17b from [2]	+	++	−	3.7
quadratic upwind	3.7 from [3]	−	+	−	2.0
cyclic	3.29 from [3]	+	++	−	1.9
MFCT	4.3 from [4]	++	+	+	2.5
limited - $\kappa = \frac{1}{3}$	5.9 from [5]	++	+	++	2.9
upwind biased ENO-6	6.2d from [6]	++	++	++	see discussion in Section 6.3 of [6]
SEM	7.6 from [7]	++	++	+	.
SGA-consistent	8.2 from [8]	++	++	+	.
adjoint-equation	9.4 from [9]	++	++	++	3.1
second-moment	10.11 from [10]	++	++	++	2.0

Table 9: Specific discretization methods and their evaluation for Problem 1.

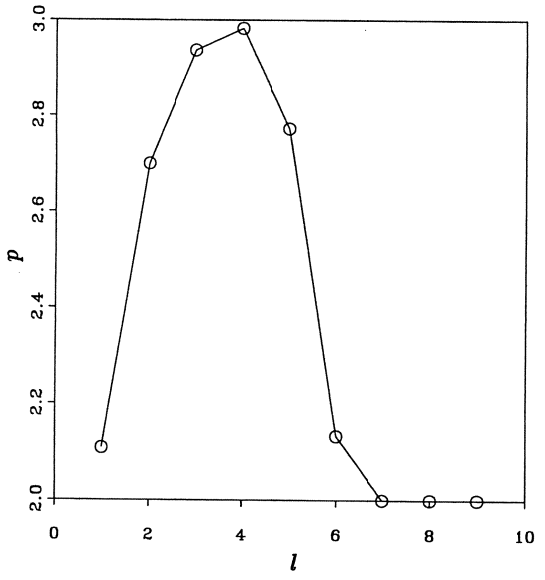

Figure 12: Orders of $\|\Delta c\|_1$-accuracy measured for Problem 1 on an extensive sequence of grids, for third-order accurate space discretization.

method	*Figure*	*maximum*	*wake*	*positivity*	$p_{\|\Delta c\|_1}$
compact RK4	2.19c from [2]	++	++	++	2.0
quadratic upwind	3.13 from [3]	+	+	++	1.9
cyclic	3.33 from [3]	++	++	+	0.6
MFCT	4.7 from [4]	++	+	+	2.6
limited - $\kappa = \frac{1}{3}$	5.13 from [5]	++	++	++	1.9
ENO-6	6.3b from [6]	++	++	++	·
SEM	7.3 from [7]	++	+	+	·
SGA	8.5 from [8]	++	+	−	·
adjoint-equation	9.6 from [9]	++	+	−	1.1
second-moment	10.12 from [10]	++	+	−	1.7

Table 10: Specific discretization methods and their evaluation for Problem 2.

[6], for the present problem Walsteijn pointed out the feature that for $\mathcal{O}(h^p)_{p>2}$ methods, after a "pre-asymptotic" convergence to their corresponding theoretical $\mathcal{O}(h^p)$ (valid for perfectly smooth problems), the orders finally converge to the expected $\mathcal{O}(h^2)$. To show this "pre-asymptotic" convergence, in Figure 12 we depict the orders of $\|\Delta c\|_1$-accuracy that we measured on a very extensive sequence of grids, by means of a finite-difference space discretization which is formally third-order accurate for the advective part (a non-limited - $\kappa = \frac{1}{3}$ discretization), and fourth-order accurate for the diffusive part (standard $\mathcal{O}(h^4)$ central). Time integration is done through the standard, fourth-order accurate Runge-Kutta scheme, with the time step Δt in linear proportion to the mesh size and sufficiently small to ensure that time discretization errors are negligible with respect to space discretization errors. In Figure 12, grid level l corresponds to the grid with $2^l \times 20$ (interior) grid points. Indeed, it appears that $\mathcal{O}(h^3)$ convergence sets in at first, but that at enhanced grid refinement, $\|\Delta c\|_1$ finally converges as $\mathcal{O}(h^2)$. It is remarkable that the "pre-asymptotic" $\mathcal{O}(h^3)$ accuracy collapses where the cell Péclet number $P = \frac{uh}{D}$ passes 1: from $l = 4$ to $l = 5$. As soon as P has become smaller than 1, for reasons of accuracy, it is expected that Δt should be taken proportional to h^2 (instead of proportional to h, as we did). A conjecture might be that not obeying this quadratic proportionality is a secondary cause of the order reduction. However, additional numerical experiments with Δt in proportion to h^2 have shown that this conjecture is false; in going from $l = 4$ to $l = 5$, the identical collapse of $p_{\|\Delta c\|_1}$ occurred. The explanation for the "pre-asymptotic" convergence to higher than $\mathcal{O}(h^2)$ accuracy is that at first, (i.e. on the coarser meshes) the kinks are not yet clearly 'visible', and hence - at first - there is no reduction of accuracy.

The present results suggest that $\mathcal{O}(h^p)_{p>2}$ discretization methods are of limited practical importance to pollutant-transport problems, since non-smooth initial solutions are very common in these problems.

3.2 Problem 2

In Table 10 (in the 3rd-5th column), the qualitative evaluation for Problem 2 is given. As far as it concerns the advective discretization, all selected methods are the same as those just evaluated for Problem 1, except for the compact RK4 scheme, which uses a compact, fourth-order accurate space discretization. For details on it we refer to [2]. In the present evaluation, we also look at qualitative solution accuracy in the wake of the source. (Uncareful treatment of the two discontinuities in the source is expected to show up in the wake.) In the last column we give again orders of accuracy with respect to $\|\Delta c\|_1$. It is to be expected that local $\mathcal{O}(h)$ errors occur near the two jumps; $\|\Delta c\|_1$ will then behave $\mathcal{O}(h^2)$ at most.

As opposed to the accuracy results observed for Problem 1 (Table 9, last column), here it appears that not till very fine, but already on the present moderately fine grids, most of the numerical methods do *not* reach higher than second-order accuracy. (Only the MFCT scheme does.) Since discontinuous source terms may also often occur in pollutant-transport problems, this probable accuracy barrier suggests that $\mathcal{O}(h^p)_{p>2}$ discretization methods might be of limited importance to these problems as well.

method	*Figure*	*phase*	*maximum*	*monotonicity*
compact RK4	2.13 from [2]	++	++	+
quadratic upwind	3.16 from [3]	+	+	−
MFCT	4.11 from [4]	++	+	+
limited - $\kappa = \frac{1}{3}$	5.5 from [5]	++	+	++
ENO-4	6.4d from [6]	++	++	++
SEM	7.7 from [7]	++	++	−
SGA	8.7 from [8]	++	++	+
adjoint-equation	9.7 from [9]	+	+	−
second-moment	10.13 from [10]	++	++	−

Table 11: Specific discretization methods and their evaluation for Problem 3.1.

method	*Figure*	*phase*	*steepness*	*monotonicity*
Lax-Wendroff	2.12 from [2]	++	++	−
first-order upwind	3.17 from [3]	++	++	−
MFCT	4.14 from [4]	++	++	+
limited - $\kappa = \frac{1}{3}$	5.6 from [5]	++	++	++
ENO-4	6.6d from [6]	++	++	++
SEM-Picard	7.8 from [7]	+	+	+
SUPG	8.9 from [8]	++	++	−
adjoint-equation	9.8+9.9 from [9]	+	+	+
second-moment	10.14 from [10]	++	++	+

Table 12: Specific discretization methods and their evaluation for Problem 3.2.

3.3 Problem 3.1

For Problem 3.1 we confine ourselves to a qualitative evaluation only (Table 11). The advection schemes to be evaluated here are all the same as those evaluated for Problem 2, except for [6], for which the standard, fourth-order accurate ENO scheme is considered. Unfortunately, no cyclic scheme has been applied to this nonlinear problem, nor to Problem 3.2. Instead of positivity we consider monotonicity. As expected, the monotonicity property has become more discriminating here than it was for the previous linear problems. The results in Table 11 speak for themselves.

3.4 Problem 3.2

In Table 12, the evaluation for Problem 3.2 is given. Basically the same schemes are evaluated as for Problem 3.1. New are the Lax-Wendroff scheme applied in [2], the standard first-order upwind scheme applied in [3] and the SUPG (streamline upwind Petrov-Galerkin scheme) applied in [8]. Except for the local maximum, the same properties are considered as for Problem 3.1. (Instead of the local maximum, we look at the steepness of the discontinuity.) The monotonicity property has become even more discriminating here.

Remarkable are the very small phase errors shown by almost all methods. As known, use of the non-conservative form of the equation may lead to erroneous shock solutions. Surprisingly, this does not even occur with the spectral-element method which is explicitly in non-conservative form. As expected, the streamline upwind Petrov-Galerkin finite-element scheme performs better for this non-smooth problem than does the standard Galerkin finite-element scheme. (We remark that the streamline upwind Petrov-Galerkin scheme applied in [7] is not a specifically tailored method, but - instead - a generally applicable method.) The unexpected monotonicity which arises in the first-order upwind results from [3], is caused by a central evaluation of the term c^4 in the quasi-linear form of the equation (see Section 3.2.4 in [3]).

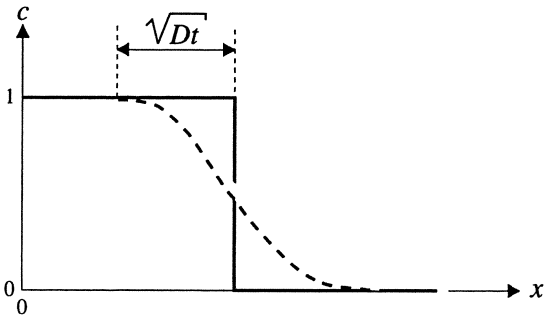

Figure 13: Exact solution and solution of first-order accurate upwind discretization; linear advection equation with discontinuous initial solution.

Because, in general, an $\mathcal{O}(1)$ solution error will occur at the shock, a higher than $\mathcal{O}(h)$ convergence of $\|\Delta c\|_1$ generally cannot be expected. Despite of this severe order barrier, the order of accuracy of discretization methods is still of some interest here. For linear shock propagation, it can be argued that a p-th order method yields an $\mathcal{O}(\frac{p}{p+1})$ $\|\Delta c\|_1$-convergence. To give some evidence of this, consider the equation

$$\frac{\partial c}{\partial t} + u\frac{\partial c}{\partial x} = 0, \tag{8}$$

with the initial solution

$$\begin{aligned} c(x, t = 0) &= 1 \quad x \leq 0, \\ c(x, t = 0) &= 0 \quad x > 0. \end{aligned} \tag{9}$$

It is known (see e.g. [13, 14]) that the standard first-order accurate upwind scheme yields a solution which approximately satisfies the modified equation

$$\frac{\partial c}{\partial t} + u\frac{\partial c}{\partial x} = D\frac{\partial^2 c}{\partial x^2}, \tag{10}$$

where $D = \mathcal{O}(h)$. Both (8) and (10) can be solved exactly. Then $\|\Delta c\|_1$ can be determined. It is found to behave as $\mathcal{O}(\sqrt{Dt})$ (Figure 13), i.e. (with $D = \mathcal{O}(h)$) as $\mathcal{O}(\sqrt{h})$. A similar reasoning for a second-order accurate space discretization leads to an $\mathcal{O}(h^{\frac{2}{3}})$ convergence of $\|\Delta c\|_1$. In general, for an $\mathcal{O}(h^p)$ space discretization and a linear shock problem, an $\mathcal{O}(1)$ error will be committed at the shock, whereas the region over which this error spreads will have an $\mathcal{O}\left(Dt\right)^{\frac{1}{p+1}}$ width. As a consequence, one gets an $\mathcal{O}\left(h^{\frac{p}{p+1}}\right)$ $\|\Delta c\|_1$-convergence. A similar analysis for the nonlinear advection equation

$$\frac{\partial c}{\partial t} + \frac{\partial (c^n)}{\partial x} = 0, \tag{11}$$

would be of interest. It might well show that for Problem 3.2, $\|\Delta c\|_1$ converges faster than $\mathcal{O}(h^{\frac{p}{p+1}})$ (but still slower than $\mathcal{O}(h)$, of course). With increasing nonlinearity, the region in which the error occurs (Figure 13) is expected to be compressed.

In conclusion, we remark that a *non-scalar* variant of this problem would have been more discriminating, for, whereas in a scalar problem numerical errors entering the shock are 'swallowed' by it, in a non-scalar problem such errors may come out of it again.

4 Conclusions

A rather wide variety of discretization methods for advection-diffusion equations has been evaluated: finite-difference, finite-volume, finite-element, spectral-element, semi-Lagrangian, and fluctuation-splitting methods; central and upwind methods; conservative and non-conservative methods; linear and nonlinear methods; and so on. Among all discretization methods considered, the "ultimate" method has not been found, though for the prescribed set of test problems a few methods come very close.

For a possible future evaluation, we suggest that test problems are prescribed which are of a more large-scale nature. We are thinking of e.g. 2-D boundary-layer problems, 2-D nonlinear advection problems, and 3-D linear advection problems. The advantage of 'large-scaleness' is the increased importance of computational efficiency. As for the present evaluation, we hope that sufficient material has been presented to select methods which meet first requirements.

Acknowledgment

J.C.H. van Eijkeren, B. van Leer, R. Struijs, and F.H. Walsteijn are acknowledged for their suggestions in improving this report.

References

[1] VREUGDENHIL, C.B.: Introduction, Chapter 1 in *Numerical Methods for Advection-Diffusion Problems, Notes on Numerical Fluid Mechanics* (Vieweg, Braunschweig, to appear).

[2] VREUGDENHIL, C.B.: Linear central finite-difference methods, Chapter 2 in —

[3] VAN EIJKEREN, J.C.H., DE HAAN, B.J., STELLING, G.S., VAN STIJN TH.L.: Linear upwind biased methods, Chapter 3 in —

[4] POURQUIÉ, M.: Some classical non-linear schemes for advection, Chapter 4 in —

[5] KOREN, B.: A robust upwind discretization method for advection, diffusion and source terms, Chapter 5 in —

[6] WALSTEIJN, F.H.: Essentially non-oscillatory (ENO) schemes, Chapter 6 in —

[7] TIMMERMANS, L.J.P., VAN DE VOSSE, F.N.: Spectral methods for advection-diffusion problems, Chapter 7 in —

[8] SEGAL, A.: Finite element methods for advection-diffusion equations, Chapter 8 in —

[9] VAN EIJKEREN, J.C.H.: Backward semi-Lagrangian methods: an adjoint equation method, Chapter 9 in —

[10] DE KOK, J.M.: Forward semi-Lagrangian methods: the second moment method, Chapter 10 in —

[11] STRUIJS, R.: The fluctuation splitting method, Chapter 11 in —

[12] KOREN, B., VREUGDENHIL, C.B.: Evaluation of the numerical results, Chapter 15 in —

[13] LEVEQUE, R.J.: *Numerical Methods for Conservation Laws* (Birkhäuser, Basel, 1990).

[14] STRIKWERDA, J.C.: *Finite Difference Schemes and Partial Differential Equations* (Wadsworth and Brooks/Cole, Pacific Grove, California, 1989).

Contents

1 Introduction **1**
1.1 Test problems 1
1.1.1 Problem 1 1
1.1.2 Problem 2 2
1.1.3 Problems 3.1 and 3.2 3
1.1.4 Problem 4 3
1.2 Discretization methods 4

2 Evaluation numerical results Problem 4 **5**
2.1 Plain accuracy 7
2.1.1 Peak resolution 7
2.1.2 L_∞-norm solution error 8
2.1.3 L_1-norm solution error 10
2.2 Accuracy versus computational efficiency 10
2.3 Positivity 12
2.4 Conservation 13
2.5 Synopsis 13

3 Evaluation numerical results Problems 1, 2, 3.1, and 3.2 **15**
3.1 Problem 1 15
3.2 Problem 2 17
3.3 Problem 3.1 18
3.4 Problem 3.2 18

4 Conclusions **20**